

TDR/DMT Characterization of a Reservoir Sediment under Water

An-Bin Huang and Chih-Ping Lin

Department of Civil Engineering, National Chiao Tung University, Hsin Chu, TAIWAN

Keywords: DMT, time domain reflectometry, sediment, in situ density, stress state

ABSTRACT: The Shihmen Reservoir, completed in early 1960's, has been an important hydro project in Northern Taiwan. Soil erosion and sediment have been a major concern for the longevity of the reservoir. After a series of typhoons in 2004, the intake valve of the hydro power plant was covered by 10m of sediment. The power generation has been halted since then. The intake valve was originally designed to be operated in clean water. In order to evaluate the feasibility of re-opening the power plant intake valve, it was necessary to know the density state of the sediment (referred to locally as the bottom mud) and the lateral pressure exerted on the intake valve. The center of the intake valve was at approximately 70m below water. A testing device that consisted of a time domain reflectometry (TDR) probe placed on top of the Marchetti dilatometer (DMT) was developed by the authors to determine simultaneously, the solid concentration, stiffness and stress state of the bottom mud. The TDR/DMT probe was attached to a string of 90m long drill rods. A skid mount drill rig bolted to a barge was used to control the drill rods. The weight of the drill rods was sufficient to push the TDR/DMT probe into the bottom mud. TDR and DMT readings were taken from 60 to 80m below water. The conductivity measurement from the TDR probe was used to determine the solid concentration. The lateral stress was inferred from the DMT P_0 readings. The difference between p_0 and p_1 was used to determine the density state of the bottom mud. Ten DMT profiles were taken, five of them had TDR readings. The paper describes field set up of the TDR/DMT probe, its test procedure and interpretation of the test results.

1 INTRODUCTION

Shihmen Reservoir is a multi-purpose water resources project, for irrigation, power generation, water supply, flood control and tourism. The Shihmen Dam is an earth-filled dam situated at approximately 50 km south east of Taipei. Since plugging of the diversion tunnel in May, 1963, the hydro-project has made significant contributions to northern Taiwan in agricultural production, industrial and economic developments, as well as alleviating flood or drought losses. The watershed of Shihmen Reservoir has characteristics of being steep in slopes and weak in geologic formations. As a result, during heavy storms, severe surface erosions coupled with land slides often occur. Since its completion in 1963, reservoir siltation has gradually increased, in spite of measures taken on dredging and construction of silt retention structures. The reservoir was designed to have a total storage of 309 million m^3 (volume of water that can be stored in the reservoir) and an effective storage of 252 million m^3 (volume of water

above the intake level). As of March of 2004, the total storage had been reduced to 253 million m^3 and the effective storage was 238 million m^3 . Aere Typhoon invaded northern Taiwan in August, 2004. The event caused an average rainfall of 973mm in the watershed which resulted in a total landslide area of 854 hectares, and an estimated inflow of approximately 28 million m^3 of sediments into the Reservoir. This has caused severe impacts on normal operation and useful life of the Reservoir. One of the immediate impacts was that the intake valve of the hydro power plant was covered by 10m of sediment. The power generation has been halted since then. The intake valve with its center at approximately 70m below water, was originally designed to be operated in clean water. In order to evaluate if the control mechanism had sufficient power to safely lift the intake valve, it was necessary to know the density state of the sediment (referred to locally as the bottom mud) and the lateral pressure exerted on the intake valve. A premature pulling of the mechanism could cause severe damage to the

forty year old intake valve. Because of the significant amount of revenue involved in power generation, the reservoir operator was eager to obtain the necessary parameters for their decision making.

The bottom mud was expected to have consistencies ranging from close to liquid to as stiff as medium dense silt. The Marchetti dilatometer (DMT) (Marchetti, 1980) with its pointed blade can easily penetrate into the bottom mud, using the weight of the drill rods. The material density, γ and its ratio to that of water, γ_w or γ/γ_w can be inferred through DMT modulus (E_D) and material index, I_D as shown in Figure 1. However, this empirical procedure is limited to γ/γ_w greater than 1.5. The time domain reflectometry (TDR) on the other hand, can be used to estimate the concentration of sediment (or density of the bottom mud) through dielectric constant and electrical conductivity measurements. The correlation between TDR readings and concentration of sediment is most desirable when γ/γ_w is less than 1.5. Thus, a combination of DMT and TDR should compliment each other and serve the purpose as a hybrid testing device.

After a brief description on the principles of TDR, the paper presents field set up of the TDR/DMT probe, the test results and their interpretation.

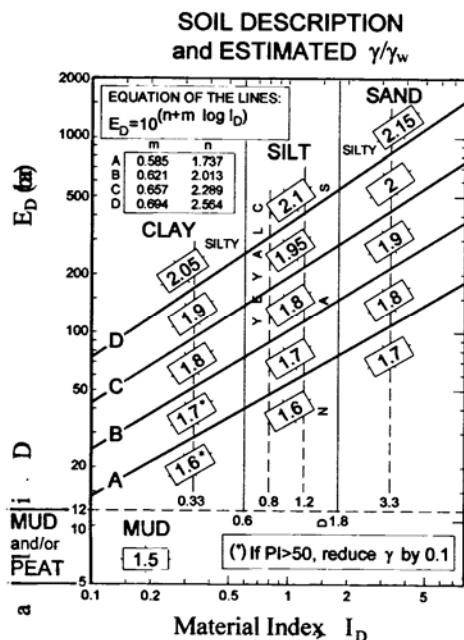


Figure 1. Soil classification and density estimation based on DMT (Marchetti and Crapps, 1981).

2 PRINCIPLES OF THE TDR

The basic principle of time domain reflectometry (TDR) is the same as radar. Instead of transmitting a 3-D wave front, the electromagnetic wave in a TDR system is confined in a waveguide. Figure 2 shows a typical TDR measurement setup composed of a TDR device and a transmission line system. A TDR device generally consists of a pulse generator, a

sampler, and an oscilloscope; the transmission line system consists of a leading coaxial cable and a measurement waveguide. The pulse generator sends an electromagnetic pulse along a transmission line and the oscilloscope is used to observe the returning reflections from the measurement waveguide due to impedance mismatches. The electromagnetic pulse is reflected at the beginning and end of the probe. The TDR waveform recorded by the sampling oscilloscope is a result of multiple reflections and dielectric dispersion. A typical TDR output waveform is shown in Figure 3. Electrical properties of the material surrounding the sensing waveguide can be determined from the TDR waveform and geometry of the waveguide (Giese and Tiemann 1975; Topp et al. 1980; Heimovaara 1994; Lin 2003).

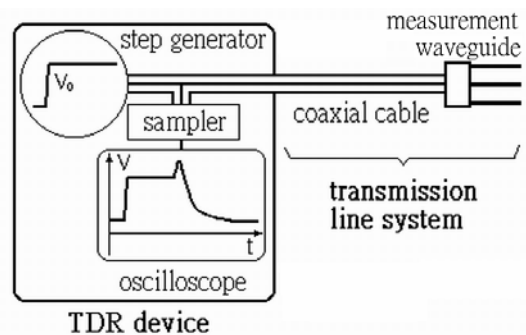


Figure 2. Typical configuration of a TDR measurement system.

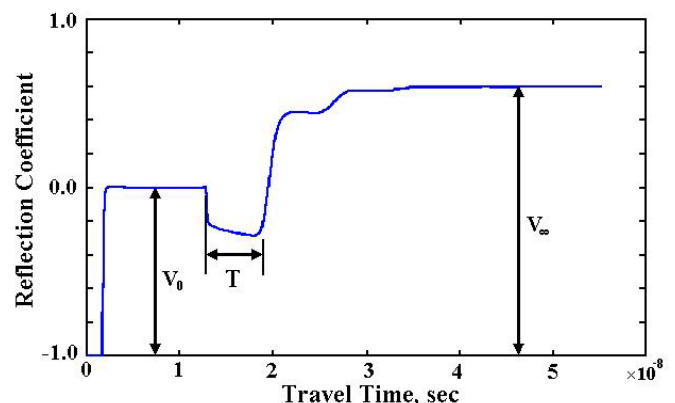


Figure 3. Determination of apparent dielectric constant and electrical conductivity from TDR signal.

The electrical properties of a material include frequency-dependent dielectric permittivity (ϵ) and electrical conductivity (σ). A travel time analysis of the two reflections can determine the apparent dielectric constant (K_a) as

$$\sqrt{K_a} = \frac{cT}{2L} \quad (1)$$

in which c is the speed of light, T is the time difference between the arrivals of the two reflections (as shown in Figure. 3) and L is the length of the sensing waveguide. The electrical conductivity (σ) can be measured using the steady-state response as

$$\sigma = \left(\frac{\varepsilon_0 c}{L} \right) \left(\frac{Z_p}{R_s} \right) \left(\frac{2V_0}{V_\infty} - 1 \right) = \alpha \left(\frac{2}{V_{r,\infty}} - 1 \right) \quad (2)$$

where ε_0 is the dielectric permittivity of free space, c is the speed of light, L is the length of the probe, Z_p is the impedance of the probe filled with air (called geometric impedance), R_s is the output impedance of the TDR device (typically 50 ohm), V_0 is the amplitude of the step input, and V_∞ is the asymptotic value of the reflected signal. To simplify the expression, $V_{r,\infty} = V_\infty/V_0$ is defined as the asymptotic value of the voltage relative to input and α is a lumped parameter accounting for geometric factors (Z_p and L) and instrument parameter (R_s). The geometric factor Z_p may be calculated theoretically from probe dimensions for probes with special configurations (Ramo et al., 1994). In practice, it is easier to calibrate the lumped parameter α with measurements in solutions of known electrical conductivity.

3 CORRELATING TDR SIGNALS TO SEDIMENT CONCENTRATION

Sediment concentration may be measured electrically based on the relationship between the sediment concentration and electrical properties. Because of the permanent dipole of the water molecule, the dielectric constant of water is very high (≈ 80 at frequencies below the water relaxation frequency). Dry soil is only polarizable by atomic and electronic polarization, leading to a low dielectric constant (typically it is less than 5). This difference makes it possible to measure the sediment concentration by determining the dielectric constant of the soil-water mixture. Sediment samples were taken from the Shihmen reservoir to conduct calibration tests for sediment concentration. Figure 4 shows the relationship between the apparent dielectric constant and sediment concentration in ppm (parts per million). The dielectric constant method is more suitable for determining high sediment concentration. When the sediment concentration is below 0.2×10^5 ppm, the dielectric constant readings tend to fluctuate significantly. A more sensitive and consistent relationship between the electrical conductivity and sediment concentration can be found, but the relationship is affected by water salinity. The experimental results reveal a unique relationship between the electrical conductivity and sediment concentration if the electrical conductivity of water phase (σ_w) is subtracted from the electrical conductivity of the soil-water mixture (σ), as shown in Figure 5. For better sensitivity, the sediment concentration is determined from electrical conductivity in this study. As shown in Figure 5, however, when sediment concentration exceeds 10×10^5 ppm, the correlation between sediment concentration and electrical conductivity curves downward and loses its linearity.

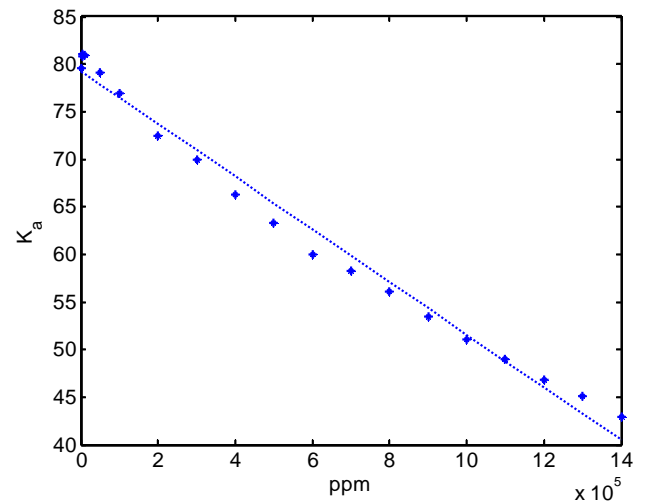


Figure 4. Relationship between dielectric constant and sediment concentration.

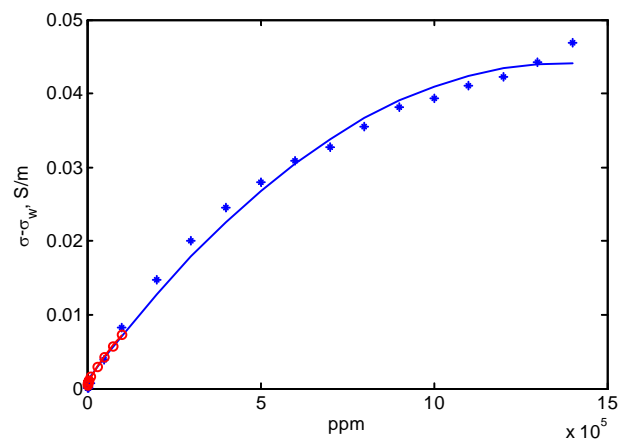


Figure 5. Relationship between electrical conductivity and sediment concentration.

4 THE TDR/DMT PROBE

A TDR penetrometer is a multi-conductor waveguide placed around a non-conductive cylindrical shaft (Lin et al., 2005a and 2005b). In this study, the TDR penetrometer module used is 800 mm long, in which the main part is a 2-conductor, 300 mm long sensing waveguide configured into a hollow, cylindrical shape as shown in Figure 6. With an outside diameter of 35.6 mm, it was designed to be used in conjunction with CPT or DMT so that the TDR waveguide can be inserted into soil at greater depths. The TDR penetrometer waveguide allows simultaneous measurement of dielectric permittivity and electrical conductivity during penetration. Unlike the conventional multi-conductor waveguide in which the conductors are fully embedded in the soil near ground surface, the TDR penetrometer waveguide is placed in between the non-conducting shaft and the surrounding soils at depths. Therefore, the TDR waveform responds not only to the surrounding material of interest but also the non-conducting shaft. The apparent dielectric constant and electrical conductivity calculated by Eqs 1 and 2 represent a weighted average of the two materials. Lin et al. (2005a and 2005b) derived a new calibra-

tion procedure for determining the electrical properties of the surrounding material. The apparent dielectric constant of the material (in this case, soil) can be written as

$$K_{a,soil} = \left(\frac{\left(\frac{cT}{2L} \right)^{2n} - b}{a} \right)^{1/n} \quad (3)$$

where n , a and b are calibration parameters for the measurement of apparent dielectric constant using the TDR penetrometer waveguide. The constants (n , a , and b) for dielectric measurements can be calibrated from TDR measurements in a few materials of known dielectric constant. Similarly, the electrical conductivity can be written as

$$\sigma_{soil} = \beta \left(\frac{2}{V_{r,\infty}} - 1 \right) \quad (4)$$

where β is the calibration parameter for measurement of electrical conductivity using the TDR penetrometer waveguide. The constant β can be calibrated from TDR measurements in a few NaCl solutions of known electrical conductivity.

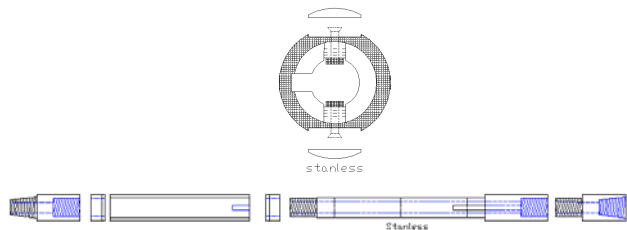


Figure 6. Schematic views of the TDR penetrometer waveguide.

In this study the TDR penetrometer waveguide was fitted immediately behind the DMT blade as shown in Figure 7. The DMT electric/pneumatic tubing passed through the inside of the hollow TDR penetrometer waveguide.



Figure 7. The TDR/DMT probe.

5 FIELD OPERATION OF TDR/DMT

The TDR/DMT probe was attached to 90 m long A rods. The A rods had a total weight of approximately 900 kg, enough to offset the buoyancy and provide reaction force to penetrate the TDR/DMT probe 10 m into the sediment. A portable drill rig mounted on a barge was used to hold the drill rods from the water surface as shown in Figure 8. The DMT tubing along with the TDR co-axial cable were threaded to the outside of the A rods through an adaptor and then connected to their respective control unit on the barge. The function of the drill rig was to hang the drill rods and passively let them be lowered instead of pushing the drill rods. Thus, the arrangement should avoid the potential problem of buckling the drill rods. The relative position of the drill rig in relation to a reference point on the dam crest was determined with a total station. The barge was fixed to a rather massive dredging boat which was in turn fixed to the shore with cables. All drainage tunnels of the reservoir were shut down during TDR/DMT tests to prevent fluctuation of the water surface elevation. With these arrangements, the barge vertical movement during a single DMT is expected to be less than 30 mm.



Figure 8. Operation of TDR/DMT from a barge.

The water surface was at an elevation of 244 m at the time of field testing. A total of 10 profiles were conducted, five of them used the TDR/DMT probe (numbered TDR/DMT-1 to TDR/DMT-5), and the other five profiles used DMT only (numbered DMT-1 to DMT-5). Figure 9 presents a location diagram of all the DMT and TDR/DMT operations. In plan view and at water surface level, the test locations were at 50 to as much as 130 m from the shore line. The power plant inlet was located on the surface of a natural rock formation with a slope of approximately 2 (vertical):1 (horizontal). The DMT readings started at elevation 185 m, TDR tests began at elevation 215, all tests ended at elevation 160 m. Thus, the bottom of the penetration could be as close as 10 m from the rock surface. The test interval varied

from 5 m in clean water to 20 cm in dense sediment. The DMT was inflated to just below A reading at all times when underwater. This arrangement prevented any possibility of water leakage and provided an opportunity to calibrate the DMT p_0 readings against the hydrostatic pressure (u_0) in clean water while lowering the DMT.

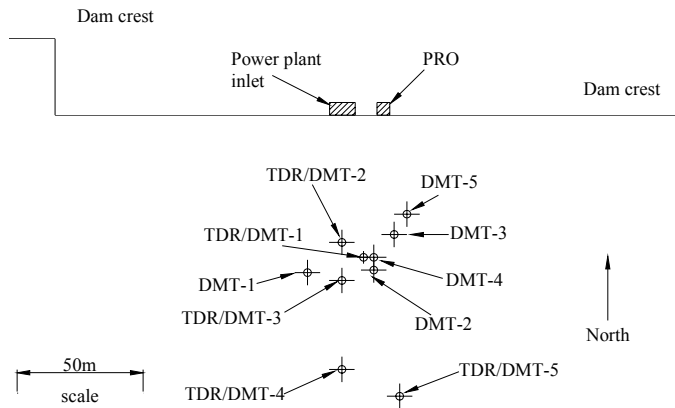


Figure 9. The test locations.

6 INTERPRETATION OF TEST RESULTS

Figure 10 shows a series of waveforms recorded in TDR/DMT-3, of reflection coefficient versus the sequential number of data points. At elevation 212.5, TDR was in clean water, the waveform at elevation 182.5 m indicated that the TDR had entered bottom mud. The depth or elevation of all the TDR and DMT was referred to the center of the DMT blade. The reflection coefficient towards the end of the record where the reading had reached a stable value was referred to as the terminal value, $V_{r,\infty}$. A laboratory calibration between $V_{r,\infty}$ and $(\sigma - \sigma_w)$ at various sediment concentrations was conducted using the sediment and water collected from the test location. With the $V_{r,\infty} - (\sigma - \sigma_w)$ correlation and relationship between $(\sigma - \sigma_w)$ and sediment concentration as shown in Figure 5, the sediment concentration in terms of ppm is inferred from $V_{r,\infty}$. The solid concentration by volume (θ_s) and thus the density ratio of bottom mud over water (γ_t/γ_w) can then be calculated based on the specific gravity of the solid.

Figure 11 shows the results from the interpretation of all the TDR readings. Except for TDR/DMT-1, the tests indicated a water/mud interface at elevation 183 m where solid concentration had a significant increase to 4×10^5 ppm. At elevation 171 m, the γ_t/γ_w reached approximately 1.4. From below elevation 171 m, the TDR readings became unstable. This is likely due to the fact that the bottom mud had become solid below that elevation, and the inevitable waving of the barge caused disturbance or cavitations within the solid mud around the TDR waveguides.

The original plan of using the chart Marchetti and Crapps (1981) to determine the bottom mud density could not materialize as in most cases, p_0 was very close to u_0 , and that resulted in unreasonable material index, I_D . Thus, the interpretation of DMT results was mostly based on p_0 and p_1 . In diluted bottom mud, where the strength was close to zero, p_0 should represent the ambient total stress. Thus a comparison between the increase of p_0 and that of hydrostatic pressure with depth should reveal the presence of mud. As the solid content continued to increase and the mud turned into solid, there should be significant differences between p_0 and p_1 and thus the E_D values can be inferred. The results of DMT-1 to DMT-5, following the above concept are shown in Figure 12. Significant differences between p_0 and u_0 could not be identified until elevation 176 m which was 7 m lower than the TDR prediction.

From below elevation 173 m, the E_D became consistently larger than zero, indicating that the bottom mud was dense enough to behave like solid. As in the case of TDR, below elevation 171 m, the E_D became erratic likely due to the solid nature of the material and wave motion of the barge.

The DMT results from TDR/DMT-1 to TDR/DMT-5 are more or less consistent with those of DMT-1 to DMT-5. Figure 13 shows the variation of DMT p_0 with elevation, based on results from TDR/DMT-1 to TDR/DMT-5 from below elevation 185 m. The total vertical stress based on γ_t of $1.1 \gamma_w$ from below elevation 176 m is also included in Figure 13. This γ_t is much lower than that suggested by TDR. The total stress based on γ_t of $1.1 \gamma_w$ fits most of the DMT p_0 data reasonably well, up to elevation 173 m. From below elevation 173 m, most of the DMT p_0 readings showed a sharp decrease. This is again likely due to the solid nature of the material and wave motion of the barge.

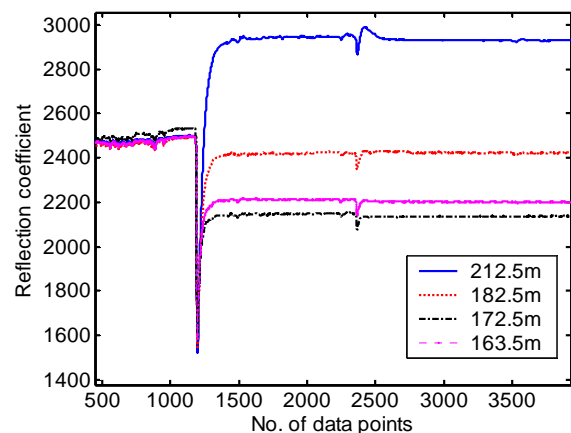


Figure 10. TDR waveforms from TDR/DMT-3.

7 CONCLUSIONS

In this project, a combination of TDR and DMT was used to investigate the interface between the clean

water and sediment as well as the density state of the sediment. Because of the diluted nature of the sediment, the TDR complimented DMT well. The experience gained in this project showed that TDR had much higher sensitivity in detecting the change of sediment or solid concentration. As a result, the interface between clean water and sediment or bottom mud according to TDR was much higher than that predicted by DMT. Also, the bottom mud density according to the change in DMT p_0 and its relationship with total vertical stress was lower than that predicted by TDR. Unless good quality samples can be taken, it is not possible to ascertain which method was more accurate. It is believed however, that much improvement in the use of DMT for similar applications can be made, if the p_0 and p_1 readings are converted into differential readings against u_0 . In this case, the interior of the DMT blade would have to be filled with water under a pressure of u_0 . The DMT has the advantage of simplicity over TDR plus the fact that DMT readings are more directly related to the stress state of the surrounding material than TDR.

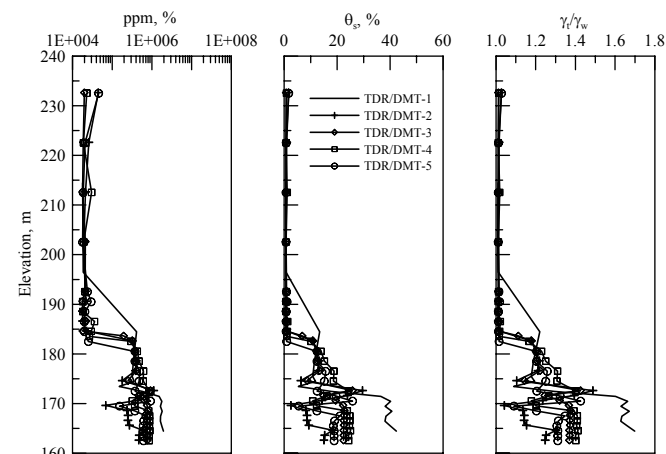


Figure 11. The interpreted TDR test results

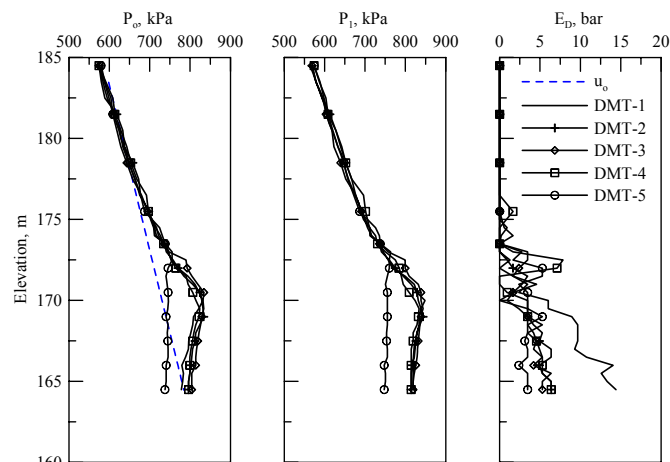


Figure 12. The DMT test results.

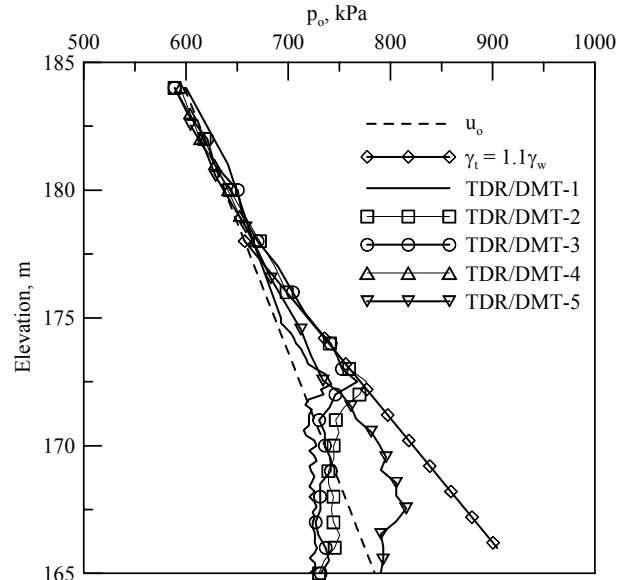


Figure 13. DMT p_0 versus elevation.

REFERENCES

Giese, K., and Tiemann, R., 1975, "Determination of the complex permittivity from thin-sample time domain reflectometry: Improved analysis of the step response wave form," *Adv. Mol. Relax. Processes*, Vol. 7, pp. 45-59.

Heimovaara, T. J., 1994, "Frequency Domain Analysis of Time Domain Reflectometry Waveforms: 1 Measurement of the Complex Dielectric Permittivity of Soils," *Water Resources Research*, Vol. 30, No. 2, pp. 189-199.

Kamey, T., and Iawasaki, K. (1995) "Evaluation of Undrained Shear Strength of Cohesive Soils Using a Flat Dilatometer," *Soils and Foundations*, Vol.35, No.2, pp.111-116.

Lin, C.-P. (2003a) "Analysis of a Non-uniform and Dispersive TDR Measurement System with Application to Dielectric Spectroscopy of Soils," *Water Resources Research*, Vol. 39, art. no. 1012.

Lin, C.-P. (2003b) "Frequency Domain versus Traveltime analyses of TDR Waveforms for Soil Moisture Measurements," *Soil Sci. Soc. Am. J.*, Vol. 67, pp.720-729.

Lin, C.-P., Chung, C.-C, and Tang, S.-H., 2005a, "Development of TDR Penetrometer through Laboratory Investigations: 1. Measurement of Soil Dielectric Permittivity," *Geotechnical Testing Journal*, submitted.

Lin, C.-P., Tang, S.-H., and Chung, C.-C, 2005b, "Development of TDR Penetrometer through Laboratory Investigations: 2. Measurement of Soil Electrical Conductivity," *Geotechnical Testing Journal*, submitted.

Marchetti, S. (1980) "In Situ Tests by Flat Dilatometer," *Journal of Geotechnical Engineering Division, ASCE*, Vol.106, No.GT3, pp.299-321.

Marchetti, S. and Crapps, D.K. (1981) "Flat Dilatometer Manual," Internal Report of G.P.E. Inc.

Ramo, S., Whinnery, J. R., and Duzer, T. V., 1994, *Fields and Waves in Communication Electromagnetics*, 3rd edition, Jown Wiley & Sons.

Topp, G. C., Davis, J. L., and Annan, A. P., 1980, "Electromagnetic Determination of Soil Water Content and Electrical Conductivity Measurement Using Time Domain Reflectometry," *Water Resources Research*, Vol. 16, pp. 574-582.